Homomorphic Wavelet-Based Statistical Despeckling of SAR Images

Stian Solbø and Torbjørn Eltoft, *Member, IEEE*

***Abstract*—In this paper, we introduce the homomorphic Γ-WMAP (wavelet maximum *a posteriori*) filter, a wavelet-based statistical speckle filter equivalent to the well known Γ-MAP filter. We perform a logarithmic transformation in order to make the speckle contribution additive and statistically independent of the radar cross section. Further, we propose to use the normal inverse Gaussian (NIG) distribution as a statistical model for the wavelet coefficients of both the reflectance image and the noise image. We show that the NIG distribution is an excellent statistical model for the wavelet coefficients of synthetic aperture radar images, and we present a method for estimating the parameters. We compare the homomorphic Γ-WMAP filter with the Γ-MAP filter and and the recently introduced Γ-WMAP filter, which are both based on the same statistical assumptions. The homomorphic Γ-WMAP filter is shown to have better performance with regard to smoothing homogeneous regions. It may in some cases introduce a small bias, but in our studies it is always less than that introduced by the Γ-MAP filter. Further, the speckle removed by the homomorphic Γ-WMAP filter has statistics closer to the theoretical model than the speckle contribution removed with the other filters.**

***Index Terms*—Homomorphic filtering, normal inverse Gaussian (NIG), synthetic aperture radar (SAR), speckle, speckle filtering, wavelet.**

I. Introduction

AS ALL COHERENT imaging systems, the synthetic aperture radar (SAR) generates images that are severely degraded by a type of multiplicative noise denoted as speckle. Speckle is caused by random interference of the backscattered electromagnetic waves due to the roughness of the imaged surface [1]. Since speckle generally tends to obscure image details, reduction of the speckle noise is important in most detection and recognition systems where speckle is present.

Over the years, a variety of techniques has been developed to despeckle images. The earliest methods were general spatial filters working directly on the intensity image using local statistics. Examples of such filters are the Lee-filter [2], the sigma-filter [3], and the Kuan-filter [4]. There also exist filters that use *a priori* statistical information about the radar cross section (RCS). The most well known example in this category is the Γ-MAP filter [5], whose name reflects that the despeckled RCS is estimated using the maximum *a posteriori* (MAP) estimation principle, assuming the underlying RCS to be Γ-distributed.

During the last decade, speckle filtering based on the wavelet transform (WT) [6] has become quite popular. Being a sparse transform, the WT has the ability to represent most of the signal energy on a relatively small number of coefficients, leaving the majority of the wavelet coefficients with values close to zero. Further, the WT is a linear transform, which implies that additive white Gaussian noise (AWGN) will remain AWGN in the wavelet domain. This makes the WT a suitable tool for removing such a noise. Usually, wavelet denoising is obtained by shrinking or thresholding the wavelet coefficients. Removing all small coefficients, while leaving the larger unchanged is referred to as hard thresholding, whereas soft thresholding also shrinks the larger coefficients toward zero [7].

Since speckle is multiplicative in nature, a common procedure is to apply denoising techniques to the wavelet coefficients of logarithmically transformed images [8]. The logarithmic transform is applied to make the speckle contribution additive, yet statistically independent of the RCS. We refer to this as *homomorphic filtering*. Many researchers report that homomorphic wavelet filtering yields better speckle reduction performance than traditional spatial speckle filters [8], [9].

There also exist several ad hoc wavelet-based filtering techniques for despeckling that can be applied directly to intensity images. One example is the method presented in [10], where all small wavelet coefficients are shrunk, as well as the large coefficients not corresponding to edges. These methods requires manual settings of thresholds and other parameters, which is a major disadvantage.

Iterative approaches to wavelet-based despeckling have also been proposed [11]–[13]. Although this type of despeckling tries to find an optimum shrinking threshold or shrinking scheme, they seldom utilize statistical assumptions about the wavelet coefficients, nor about the intensity. This is a drawback in cases where good statistical models exist. Furthermore, *a priori* information is usually not considered. This is also the case for the homomorphic wavelet filters utilizing some sort of wavelet coefficient thresholding scheme.

The authors have recently introduced the Γ-WMAP (wavelet maximum *a posteriori*) filter [14], a statistical wavelet domain speckle filter, equivalent to the classical Γ-MAP filter. The speckle contribution was modeled as additive noise, statistically dependent of the RCS. The Γ-WMAP filter was shown to have an overall good performance, but with a rather high degree of blurring. This is explained by the fact that the statistical dependence makes large wavelet coefficients associated with speckle

Manuscript received August 20, 2002; revised November 11, 2003. This work was supported in part by the European Community, Environment and Sustainable Development Programme under Contracts EVG1-CT-2001-00052 EnviSnow and EVG1-CT-2002-00085 FloodMan, and in part by the Norwegian Research Council under Contract 143540/431.

S. Solbø was with the Department of Physics, University of Tromsø, N9037 Tromsø, Norway. He is now with Norut Information Technology Ltd., N9291 Tromsø, Norway (e-mail: stian@itek.norut.no).

T. Eltoft is with the Department of Physics, University of Tromsø, N9037 Tromsø, Norway (e-mail: pcte@phys.uit.no).

Digital Object Identifier 10.1109/TGRS.2003.821885

only and, therefore, shrunk heavily toward zero. The Γ-WMAP filter applies the same filtering strategy as the wavelet-based speckle filter described in [15], which is a MAP filtering in the wavelet domain assuming beta-complex (Pearson, type IV) distributed wavelet coefficients. The major differences between the filters in [14] and [15] are the statistical models for the wavelet coefficients and the methods for estimating the statistical parameters. Further, the filter proposed in [15] replaces a pixel with its spatial average whenever the local degree of variation is below a certain limit, whereas the filter presented in [14] performs all the filtering in the wavelet domain. There have also been developed other statistical wavelet-based speckle filters, like the one proposed in [16], which performs minimum-mean-square-error filtering in the wavelet domain. This filter does not assume any statistical model for the RCS, but calculates all parameters from the estimated speckle variance.

In this paper, we develop the homomorphic Γ-WMAP filter, a statistical homomorphic wavelet domain speckle filter that is based on the same statistical assumptions as the Γ-MAP filter. That is, we assume the RCS to be Γ-distributed and that the speckle contribution is statistical independent of the RCS and follows an exponential distribution [17]. The actual filtering is performed by applying the MAP filtering principle to the wavelet coefficients of a logarithmically transformed SAR image. This implies that we need closed-form expressions for the distributions of the wavelet coefficients corresponding to both the reflectance and speckle images. We propose to use the normal inverse Gaussian (NIG) distribution [18] as a statistical model for the wavelet coefficients. This distribution is uniquely defined by four parameters. We describe how optimally fitted NIG models may be obtained in the wavelet domain by estimating the four lower order cumulants in the image domain, assuming the image intensity to be K-distributed [19], [20], and transforming the cumulants to the wavelet domain. In this way, we enable a direct relationship between the statistical models for the RCS and the wavelet coefficients.

Homomorphic speckle filtering, performed by thresholding the wavelet coefficients of log-transformed SAR images, has the problem of introducing bias [12], [21]. This is due to the fact that the logarithmic transform is nonlinear and hence results in uneven filtering. This bias is generally not available, although there has been made some attempts to analyze it [22]. The estimation of parameters from log-transformed SAR images is also problematic [23], [24]. Since the homomorphic Γ-WMAP filter presented in this paper shrinks the wavelet coefficients according to a statistical criterion, instead of strictly thresholding the wavelet coefficients, the results should not be severely degraded by bias. This hypothesis is verified by the results shown in Section IV. Further, all parameters are estimated directly from the intensity image prior to the logarithmic transformation.

Comparing our new homomorphic filter with the Γ-MAP and the Γ-WMAP filters shows that it has slightly better speckle reduction performance on homogeneous regions. Further, the statistics of the removed speckle contribution are closer to the theoretical values than the speckle contributions removed with the other two filters. However, in some cases, the homomorphic Γ-WMAP filter may introduce a bias of the same order of magnitude as the Γ-MAP, which is a larger bias than the Γ-WMAP filter introduces.

The outline of this paper is as follows. In Section II, we present some basic wavelet theory, with focus on the so-called stationary wavelet transform. Next, in Section III, we review the NIG-distribution and the estimators used for estimating its parameters. Section IV presents a statistical model for speckled SAR images and shows how this can be transformed to a model for the wavelet coefficients. Furthermore, we demonstrate the goodness of fit of this model for wavelet-transformed synthetic SAR data. We review the standard Γ-MAP statistical wavelet filter and introduce the homomorphic Γ-WMAP filter in Section V. In Section VI, we present some results on despeckling real SAR images. Finally, in Section VII, we give some conclusions.

II. Some Wavelet Transform Preliminaries

During the last decades, the WT has become a popular and useful tool in the area of signal and image processing. One of its main features is its ability to perform multiresolution decomposition. The WT does this by projecting a signal $f(x)$ onto nested subspaces $\mathbf{V}_j$ of $L^2(\mathbb{R})$ that represent approximations $f_j(x)$ of the signal at different resolutions. As a result the wavelet decomposition gives a simultaneous spatial-frequency representation.

We denote $\phi(x)$ as a *scale function* if the family $\{\phi(x-k)\}_{k\in\mathbb{Z}}$ is a Riesz basis of the space $\mathbf{V}_0$ containing the original functions. Further, we denote $\mathbf{W}_j$ a space complementing $\mathbf{V}_j$ in $\mathbf{V}_{j-1}$, i.e., that satisfies $\mathbf{V}_{j-1} = \mathbf{V}_j \oplus \mathbf{W}_j$. This space contains the details $\tilde{f}_j(x)$ that are present in $f_{j-1}(x)$ but vanish in the coarser approximation $f_j(x)$. A function ψ is called a mother wavelet if the family of functions $\{\psi(x-k)\}_{k\in\mathbb{Z}}$ is a basis for the detail space $\mathbf{W}_1$. The basis functions $\psi_{j,k}$ of the detail space $\mathbf{W}_j$ at an arbitrary level j, are found from dilating and translating the mother wavelet function $\psi_{j,k}(x) = \sqrt{2^{-j}}\psi(2^{-j}x-k)$. Likewise, the basis functions of $\mathbf{V}_j$ can be expressed as $\phi_{j,k}(x) = \sqrt{2^{-j}}\phi(2^{-j}x-k)$. These basis functions enable us to express any detail $\tilde{f}_j(x)$ or approximation $f_j(x)$ in terms of wavelet coefficients $\mathbf{d}_j$ or scale coefficients $\mathbf{a}_j$, respectively

$$f_j(x) = \sum_k a_j[k]\phi_{j,k}(x) \quad \tilde{f}_j(x) = \sum_k d_j[k]\psi_{j,k}(x). \quad (1)$$

With this formalism, all functions $f \in L^2(\mathbb{R})$ can be decomposed in the following way:

$$f(x) = \sum_k a_J[k]\phi_{J,k}(x) + \sum_{j\le J}\sum_k d_j[k]\psi_{j,k}(x). \quad (2)$$

A discrete WT (DWT) can be implemented using an iterated two channel filter bank tree as shown in Fig. 1. This is also known as the pyramidal algorithm. Lowpass filtering $a_{j-1}[n]$ with a filter $h[n]$ gives the scale coefficients $a_j[n]$ of the signal at level j. Similarly, highpass filtering $a_{j-1}[n]$ with $g[n]$ gives the wavelet coefficients $d_j[n]$. Subsampling is performed at each stage in the filter bank tree in order to keep the number of coefficients constant through the whole decomposition scheme. The relationship between the filters incorporated in the filter bank

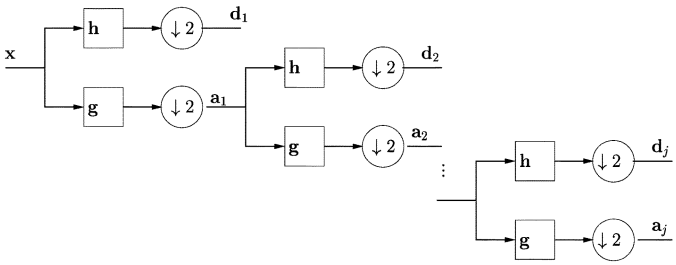

Fig. 1. Filter bank tree implementing the DWT.

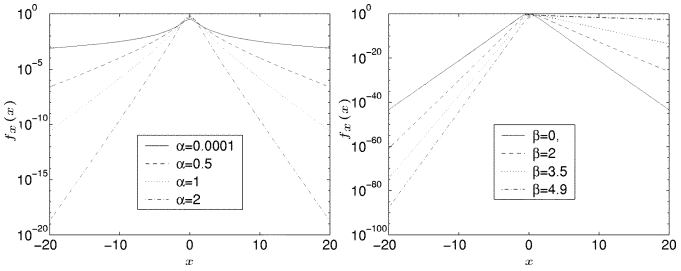

Fig. 2. (a) NIG density for different values of α, with $\beta = \mu = 0$ and $\delta = 1$. (b) NIG density for different values of β, with $\alpha = 5$, $\delta = 1$, and $\mu = 0$.

and the scale and wavelet functions are given by the following dilation equations [25]:

$$\phi(x) = \sum h[n]\phi(2x - n) \quad \psi(x) = \sum g[n]\phi(2x - n). \quad (3)$$

As a consequence of the subsampling operations in the pyramidal algorithm, the DWT does not preserve translation invariance. This means that a translation of the original signal does not necessarily imply a translation of the corresponding wavelet coefficients. The stationary wavelet transform (SWT) [26] is a special version of the DWT that has preserved translation invariance. Instead of subsampling, the SWT utilizes recursively dilated filters in order to halve the bandwidth from one level to another. At scale 2^j the filters are dilated by inserting 2^{j-1} zeros between the filter coefficients of the prototype filters. Thus, the lowpass filter $h_j[n]$ and highpass filter $g_j[n]$ at level j are given by

$$h_j[n] = \begin{cases} h\left[\frac{n}{2}\right], & n = 2^j m,\ m \in \mathbb{Z} \\ 0, & \text{else} \end{cases}$$
$$g_j[n] = \begin{cases} g\left[\frac{n}{2}\right], & n = 2^j m,\ m \in \mathbb{Z} \\ 0, & \text{else.} \end{cases} \quad (4)$$

For images, the following filter equations are used to obtain wavelet coefficients $\mathbf{D}_{j+1}$ at level $j+1$ from scale coefficients $\mathbf{A}_j$ at level j

$$A_{j+1}[x,y] = \sum_{k,l} h_j[k]h_j[l]A_j[x-k, y-l] = [\mathbf{H}_j\mathbf{A}_j]_{x,y}$$
$$D^h_{j+1}[x,y] = \sum_{k,l} g_j[k]h_j[l]A_j[x-k, y-l] = \left[\mathbf{G}^h_j\mathbf{A}_j\right]_{x,y}$$
$$D^v_{j+1}[x,y] = \sum_{k,l} h_j[k]g_j[l]A_j[x-k, y-l] = \left[\mathbf{G}^v_j\mathbf{A}_j\right]_{x,y}$$
$$D^d_{j+1}[x,y] = \sum_{k,l} g_j[k]g_j[l]A_j[x-k, y-l] = \left[\mathbf{G}^d_j\mathbf{A}_j\right]_{x,y}$$

where $[x, y]$ are the pixel coordinates. The wavelet coefficient matrices $\mathbf{D}^h_j$, $\mathbf{D}^v_j$, and $\mathbf{D}^d_j$ correspond to image details with horizontal, vertical, and diagonal orientations, respectively.

To simplify the derivation of the cumulants of the wavelet coefficients in Section IV, we introduce a compact notation to compute the stationary wavelet coefficients at an arbitrary level j. We find the stationary wavelet coefficients at level j directly from the original image $\mathbf{A}_0$ by defining the filtering operator $\mathbf{W}^\xi_j$ such that $\mathbf{D}^\xi_j = \mathbf{W}^\xi_j\mathbf{A}_0$, $\xi \in \{h, v, d\}$. This operator is the result of j successive convolutions

$$\mathbf{W}^\xi_j = \begin{cases} \mathbf{G}^\xi_0, & j = 1 \\ \mathbf{G}^\xi_{j-1}\prod_{i=0}^{j-2}\mathbf{H}_i, & j \geq 2 \end{cases}, \qquad \xi \in \{v, h, d\}. \quad (5)$$

Thus, we can express the wavelet coefficients at level j and orientation ξ corresponding to pixel $[x, y]$ as

$$D^\xi_j[x,y] = \left[\mathbf{W}^\xi_j\mathbf{A}_0\right]_{x,y} = \left(\psi^\xi_j[k,l] * A_0[k,l]\right)_{x,y} \quad (6)$$

where $*$ is the two-dimensional convolution operator, and $\psi^\xi_j[k,l]$ is the wavelet filter at level j and orientation $\xi \in \{v, h, d\}$.

III. Normal Inverse Gaussian Distribution

The *normal inverse Gaussian* (NIG) distribution is a variance-mean mixture of a Gaussian density with an inverse Gaussian density. Although this probability distribution was originally introduced as a model for data from empirical finance [27], it has recently gained popularity in the electrical engineering community. This is mainly due to its ability to model super-Gaussian processes. In many cases, it outperforms the α-stable distributions, which are commonly used to model heavy tailed data.

The stochastic variable X is said to be normal inverse Gaussian distributed, i.e., $X \sim \text{NIG}(\boldsymbol{\theta})$, if it has a probability density function (pdf) of the form [18]

$$f_X(x;\boldsymbol{\theta}) = \frac{\alpha\delta}{\pi}\frac{\exp\{p(x)\}}{q(x)}K_1[\alpha q(x)] \quad (7)$$

where K_1 is the modified Bessel function of the second kind with index 1, $p(x) = \delta\sqrt{(\alpha^2 - \beta^2)} + \beta(x - \mu)$ and $q(x) = \sqrt{(x-\mu)^2 + \delta^2}$. The shape of the NIG-density is specified by the four-dimensional parameter vector $\boldsymbol{\theta} = [\alpha, \beta, \delta, \mu]^T$, which is bound in the following way: $0 \leq |\beta| < \alpha$, $\delta > 0$ and $-\infty < \mu < \infty$. This flexible parameterization makes it possible to model a large variety of unimodal data with various decay rates of the tail. The α-parameter controls the steepness of the density, which increases monotonically with increasing α. If $\beta = 0$, the density is symmetric around the centrality parameter μ, whereas a positive or negative β corresponds to a density skewed to the right or to the left, respectively. In Fig. 2,

the influence of the parameters α and β is shown. The δ-parameter is a scale parameter and is not directly related to the overall shape of the density.

In [28], statistically consistent cumulant-based estimators for the NIG parameters are derived. By estimating the four lower order cumulants $\kappa^{(1)}$, $\kappa^{(2)}$, $\kappa^{(3)}$, and $\kappa^{(4)}$ from sample data and using these to estimate skewness $\hat{\gamma}_3 = \hat{\kappa}^{(3)}/[\hat{\kappa}^{(2)}]^{3/2}$ and normalized kurtosis $\hat{\gamma}_4 = \hat{\kappa}^{(4)}/[\hat{\kappa}^{(2)}]^2$, we form the auxiliary variables

$$\xi = 3\left(\hat{\gamma}_4 - \frac{4}{3}\hat{\gamma}_3^2\right)^{-1} \qquad \rho = \frac{\hat{\gamma}_3}{3}\sqrt{\xi}. \tag{8}$$

Thereafter, the parameter estimators can be shown to be [28]

$$\begin{aligned} \hat{\delta} &= \sqrt{\hat{\kappa}^{(2)}\xi(1-\rho^2)} & \hat{\alpha} &= \frac{\xi}{\hat{\delta}\sqrt{1-\rho^2}} \\ \hat{\beta} &= \hat{\alpha}\rho & \hat{\mu} &= \hat{\kappa}^{(1)} - \rho\sqrt{\hat{\kappa}^{(2)}\xi}. \end{aligned} \tag{9}$$

The NIG distribution can model data satisfying the following relationship between skewness and kurtosis [28]:

$$\gamma_4 \geq \frac{4\gamma_3^2}{3}. \tag{10}$$

This relationship can be derived directly from the parameter constraint $0 \leq |\beta| \leq \alpha$. For data that do not satisfy the above relationship, the cumulant-based estimators yield complex parameters. This can be used as an internal validation test of the estimators, i.e., if we estimate complex parameters from a (large enough) dataset, the data is certainly not NIG-distributed!

IV. Statistical Modeling of SAR Images

A. Image Domain Modeling

For single-look SAR images, the observed intensity $I[x, y]$ in pixel $[x, y]$ may be expressed as

$$I[x, y] = \sigma[x, y]r^2[x, y] \tag{11}$$

where σ is the RCS of the imaged surface, and the random factor r^2 represents the speckle noise, which is statistically independent of σ. For a given σ, the observed intensity in an L-look image is Γ-distributed with the following pdf:

$$f_{I|\sigma}(I|\sigma) = \left(\frac{L}{2\sigma}\right)^L \frac{I^{L-1}}{\Gamma(L)} e^{-LI/2\sigma}. \tag{12}$$

For single-look SAR images this reduces to an exponential distribution

$$f_{I|\sigma}(I|\sigma) = \frac{1}{2\sigma} e^{-I/2\sigma}. \tag{13}$$

The RCS is often assumed to be Γ-distributed, i.e.,

$$f_\sigma(\sigma) = \frac{\nu^\nu}{\mu_\sigma^\nu \Gamma(\nu)} \sigma^{\nu-1} e^{-\nu\sigma/\mu_\sigma} \tag{14}$$

where $\mu_\sigma = E\{\sigma\}$ and the degree of homogeneity is measured by $\nu = \mu_\sigma^2/\text{var}\{\sigma\}$. The Γ-distribution is a widely used statistical model for the RCS, e.g., for ocean SAR imagery [17]. Further, this distribution yields a pdf for the observed intensity I with a closed-for expression, namely the K-distribution [17]

$$\begin{aligned} f_I(I) &= \int f_{I|\sigma}(I|\sigma) f_\sigma(\sigma) d\sigma \\ &= \frac{2}{I\Gamma(\nu)\Gamma(L)} \left(\frac{L\nu I}{\mu_\sigma}\right)^{(L+\nu)/2} K_{\nu-L}\left(2\sqrt{\frac{L\nu I}{\mu_\sigma}}\right). \end{aligned} \tag{15}$$

The pdf of the SAR image intensity of homogeneous or textured terrain can be well modeled by the K-distribution for a wide range of scattering situations [29]. Another way of deriving this statistical model is to use the negative binomial distribution as a model for the random number of independent scatterers within each resolution cell [20], [30].

In this paper, we have assumed that the intensity images are K-distributed and have used an EM-estimator [33] to estimate the parameters μ_σ and ν. There are several other estimators that can be used to estimate the parameters μ_σ and ν from a K-distributed intensity image. Some estimators are based on the maximum-likelihood principle [31]–[33], whereas others are based, for example, on a neural network implementation [34]

B. Wavelet Domain Modeling

Speckle suppression trough wavelet coefficient shrinkage is based on the linear property of the WT. This implies that the speckle contribution must be expressed as an additive term. As indicated earlier, this will be accomplished by applying a logarithmic transformation on the observed intensity image. In the logarithmic domain, we express the observed intensity as

$$Y = X + N \tag{16}$$

where $Y = \ln I$, $X = \ln\sigma$ and $N = \ln r^2$. The logarithmic transformed RCS will have the following pdf:

$$\begin{aligned} f_X(X) &= f_\sigma(\sigma)\left|\frac{d\sigma}{dX}\right| = \frac{\nu^\nu}{\mu_\sigma^\nu\Gamma(\nu)}\sigma^{\nu-1}e^{-\nu\sigma/\mu_\sigma}|\sigma| \\ &= \frac{\nu^\nu}{\mu_\sigma^\nu\Gamma(\nu)} e^{X\nu} e^{-\nu e^X/\mu_\sigma}. \end{aligned} \tag{17}$$

Similarly, the logarithmic transformed speckle contribution will have the pdf

$$f_N(N) = f_{r^2}(r^2)\left|\frac{dr^2}{dN}\right| = \left(\frac{Le^N}{2}\right)^L \frac{e^{-Le^N/2}}{\Gamma(L)} \tag{18}$$

and this density is independent of the parameters μ_σ and ν, as expected.

In the wavelet domain, the wavelet coefficients of the log-transformed intensity image can be expressed as

$$w_Y[x, y] = w_X[x, y] + w_N[x, y] \tag{19}$$

where $w_X[x,y]$ and $w_N[x,y]$ are the wavelet coefficient images corresponding to the reflectance image $\sigma[x,y]$ and the speckle image $r^2[x,y]$, respectively.

In this paper, we apply the stationary wavelet transform, because this enables us to express the cumulants in the wavelet domain in terms of the cumulants in the image domain. Since the SWT is a sparse transform, it is more probable that a given wavelet coefficient has a value close to zero, than a large one. This implies that the wavelet coefficients should be modeled with a unimodal distribution. Further, wavelet coefficients are generally observed to be heavy-tailed; thus, the statistical model should be non-Gaussian [35].

We now fit NIG-distributions to both the wavelet coefficients of the reflectance image and the wavelet coefficients of the noise image, i.e., $w_X[x,y] \sim \text{NIG}(\boldsymbol{\theta}_X)$ and $w_N[x,y] \sim \text{NIG}(\boldsymbol{\theta}_N)$, with $\boldsymbol{\theta}_X$ and $\boldsymbol{\theta}_N$ being parameter vectors containing the parameters of the respective NIG-distributions. Furthermore, according to the results in Section III, these parameters are uniquely specified from the first four lower order cumulants of the corresponding wavelet coefficient images.

In [15], it was shown that the relationship between the nth-order cumulants of an image $I[x,y]$, and the corresponding cumulants of the coefficients obtained by an SWT of $I[x,y]$ can be expressed as

$$\kappa^{(n)}_{w^{\xi}_{I,j}} = \sum_{k,l} \left(\psi^{\xi}_j[k,l]\right)^n \kappa^{(n)}_I \tag{20}$$

where $w^{\xi}_{I,j}$ are the wavelet coefficients on scale 2^j corresponding to orientation $\xi \in \{h,v,d\}$. Further, the sum in the above relation can be expressed as [15]

$$\sum_{k,l}\left(\psi^{\xi}_j[k,l]\right)^n = \begin{cases} \left(\sum_k (g[k])^n\right)\left(\sum_l (h[l])^n\right)^{2j-1}, & \xi \neq d \\ \left(\sum_k (g[k])^n\right)^2\left(\sum_l (h[l])^n\right)^{2(j-1)}, & \xi = d. \end{cases} \tag{21}$$

This implies that we only need to estimate the cumulants of the logarithmically transformed RCS and speckle images to find the NIG models of the wavelet coefficients.

It is not possible to derive analytical expressions for the cumulants of $X[x,y]$, nor the cumulants of $N[x,y]$ in terms of the parameters μ_σ and ν. For the log-transformed RCS, the cumulants can be computed from the cumulant-generating function

$$\begin{aligned}\Phi_X(s) &= \ln\left\{\int_{-\infty}^{\infty} f_X(X) e^{-jsX} dX\right\} \\ &= \ln\left\{\int_0^{\infty} \left(\frac{\nu}{\mu_\sigma}\right)^{\nu} \frac{1}{\Gamma(\nu)} e^{X\nu} e^{-\frac{\nu e^X}{\mu_\sigma}} e^{-jsX} dX\right\}\end{aligned} \tag{22}$$

which has no closed-form expression and, therefore, has to be calculated numerically. The cumulants of the log-transformed speckle can be computed from knowledge about its statistical moments. The n-order moments are given by the following equation:

$$m^{(n)}_N = \int_0^{\infty} N^n \left(\frac{Le^N}{2}\right)^L \frac{e^{-Le^N/2}}{\Gamma(L)} dN. \tag{23}$$

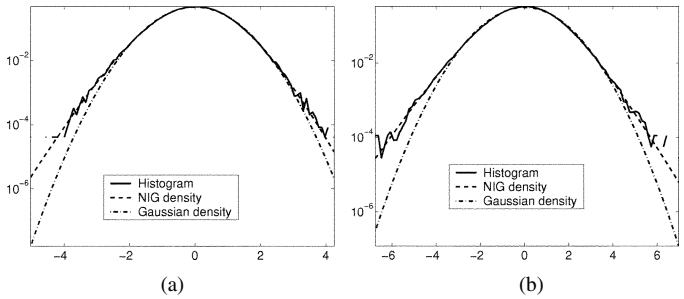

Fig. 3. NIG models fitted to the wavelet coefficients of (a) log-transformed Γ-distributed data and (b) log-transformed single-look speckle noise. Best fitted Gaussian densities are shown for comparison.

Using the four lower order statistical moments of N, we can estimate the four lower order cumulants using the following relations [36]:

$$\begin{aligned}\kappa^{(1)}_N &= m^{(1)}_N \\ \kappa^{(2)}_N &= m^{(2)}_N - \left(m^{(1)}_N\right)^2 \\ \kappa^{(3)}_N &= m^{(3)}_N - 3m^{(1)}_N m^{(2)}_N + 2\left(m^{(1)}_N\right)^3 \\ \kappa^{(4)}_N &= m^{(4)}_N - 3\left(m^{(2)}_N\right)^2 - 4m^{(1)}_N m^{(3)}_N \\ &\quad + 12\left(m^{(1)}_N\right)^2 m^{(2)}_N - 6\left(m^{(1)}_N\right)^4.\end{aligned} \tag{24}$$

Substituting the cumulants for X and N in (20), we can easily find the corresponding cumulants in the wavelet domain, and from these obtain estimates of the parameters of the best fitted NIG-distributions using the cumulant-based estimators in (9).

We observe that the statistical moments for the logarithmically transformed speckle will be independent of the RCS. Thus, the best fitted NIG model for the speckle wavelet coefficients will be global for each level and direction in the SWT decomposition.

C. Evaluating the Goodness of Fit of the Wavelet Domain Models

We now examine how well the proposed NIG models fit to the distributions of the wavelet-transformed images of $X[x,y]$ and $N[x,y]$, respectively. Since neither of these distributions are available for real SAR images, the tests are based on simulated data. The results shown in this section are based on synthetic data where the Γ-distributed RCS was generated with parameters $\mu_\sigma = 5$ and $\nu = 1.8$. In Fig. 3, a log-plot of the NIG-densities fitted to the distributions of the wavelet coefficients is shown along with the normalized histograms. We note that the curves follow each other extremely well, giving a first indication of a good data fit. Further, we see that the NIG-distributions give a much better fit than the Gaussian distributions, especially in the tails.

Another common method for evaluating the pertinence of a probability density model is to make a variance stabilized p–p plot [37]. This is done by comparing inverse sine-transformed uniformly constructed percentiles of the data with inverse sine-transformed percentiles of the proposed density. A linear curve indicates a prefect fit. In Fig. 4, stabilized p–p plots of the NIG models for $w_\sigma[x,y]$ and $w_N[x,y]$ are shown. These plots are

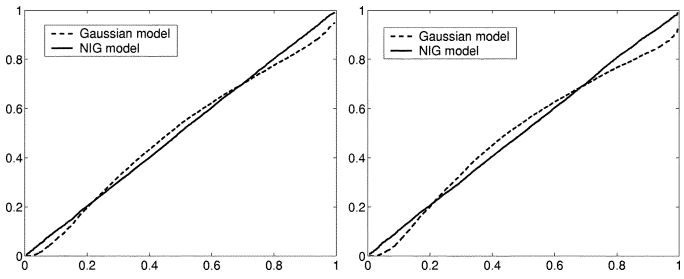

(a) (b)

Fig. 4. Variance-stabilized p–p plot for the wavelet coefficients of (a) log-transformed Γ-distributed data and (b) log-transformed speckle noise. Gaussian model shown for comparison.

very close to linear, confirming that the NIG-density is an excellent model for the wavelet coefficients of both the log-transformed reflectance image $X[x,y]$ and the log-transformed noise image $N[x,y]$. We further observe that the Gaussian distribution is too light in the tails to give good data fit. This confirms that heavy tailed distributions are needed as statistical models for the wavelet coefficients.

V. Statistical Despeckling

A. Despeckling in the Image Domain (Γ-MAP)

We will first review the classical Γ-MAP filter. This filter estimates the intensity that is most likely to occur in a speckle-free image, given the intensity in the observed image. This is known as MAP filtering and is stated in mathematical terms as

$$\hat{\sigma}_{\mathrm{MAP}} = \arg\max_{\sigma} f_{\sigma|I}(\sigma|I). \tag{25}$$

The pdf $f_{\sigma|I}(\sigma|I)$ is generally not known, but can be expressed in terms of known pdfs using Bayes rule

$$f_{\sigma|I}(\sigma|I) = \frac{f_{I|\sigma}(I|\sigma)\cdot f_{\sigma}(\sigma)}{f_I(I)}. \tag{26}$$

We find $\hat{\sigma}_{\mathrm{MAP}}$ by maximizing $f_{\sigma|I}(\sigma|I)$. This is equivalent with finding $(\partial/\partial\sigma) f_{\sigma|I}(\sigma|I) = 0$. Since the logarithmic function is monotonous, the MAP estimate can be found by considering

$$\begin{aligned}\frac{\partial}{\partial\sigma}\ln f_{\sigma|I}(\sigma|I) &= \frac{\partial}{\partial\sigma}\ln\frac{f_{I|\sigma}(I|\sigma)\cdot f_{\sigma}(\sigma)}{f_I(I)} \\ &= \frac{\partial}{\partial\sigma}\left[\ln f_{I|\sigma}(I|\sigma) + \ln f_{\sigma}(\sigma)\right]\end{aligned} \tag{27}$$

which gives the following expression for the MAP estimate:

$$\hat{\sigma}_{\mathrm{MAP}} : \frac{\partial}{\partial\sigma}\left[\ln f_{I|\sigma}(I|\sigma) + \ln f_{\sigma}(\sigma)\right]\Big|_{\sigma=\hat{\sigma}_{\mathrm{MAP}}} = 0. \tag{28}$$

Assuming the Γ-distributed model for the RCS, an L-look image yields the following quadratic equation for $\hat{\sigma}_{\mathrm{MAP}}$ [19]

$$\frac{\nu}{\mu_\sigma}\hat{\sigma}^2_{\mathrm{MAP}} - (\nu - L - 1)\hat{\sigma}_{\mathrm{MAP}} - \frac{LI}{2} = 0 \tag{29}$$

where the solution can be expressed as

$$\hat{\sigma}_{\mathrm{MAP}} = \frac{\mu_\sigma(\nu - L - 1) + \sqrt{\mu_\sigma^2(\nu - L - 1)^2 + 2\nu\mu_\sigma LI}}{2\nu}. \tag{30}$$

This is for obvious reasons referred to as a Γ-MAP filter. For improved performance on homogeneous regions and better preservation of strong scatters, edges, and other significant details, two thresholds are usually implemented in the Γ-MAP filter [5]. Consider the normalized local standard deviation

$$C_I[x,y] = \frac{s_I[x,y]}{\hat{I}[x,y]} \tag{31}$$

where $s_I[x,y]$ and $\hat{I}[x,y]$ are the standard deviation and mean in a neighborhood around pixel $[x,y]$, respectively. Then, the Γ-MAP filtering would be performed on a pixel-by-pixel basis by computing

$$\hat{\sigma} = \begin{cases} \hat{I}, & C_I < C_u \\ \hat{\sigma}_{\mathrm{MAP}}, & C_u \le C_I \le C_{\max} \\ I, & C_I > C_{\max} \end{cases} \tag{32}$$

where $C_u = 1/\sqrt{L}$ and $C_{\max} = \sqrt{2}C_u$.

We mention that, for all speckle filters, better results can be obtained by using adaptive window sizes, and supplementary detection of edges or homogeneous regions within the analysis window [38]. However, in this paper, we will use the basic version of the Γ-MAP filter, as in (32), since we focus on comparison between the Γ-MAP filter and the wavelet-based methods.

B. Despeckling in the Wavelet Domain

We derive the wavelet-based despeckling algorithm based on the same principles as the Γ-MAP filter. That is, we want to estimate the wavelet coefficient $\hat{w}_X[x,y]$ that is most likely true in a speckle-free reflectance image $\sigma[x,y]$, given a wavelet coefficient $w_Y[x,y]$ corresponding to a logarithmically transformed intensity image $Y[x,y]$. This is stated in mathematical terms as

$$\hat{w}_X = \arg\max_{w_X} f_{w_X|w_Y}(w_X|w_Y). \tag{33}$$

Using Bayes rule to obtain expressions in terms of known pdfs, we obtain

$$f_{w_X|w_Y}(w_X|w_Y) = \frac{f_{w_Y|w_X}(w_Y|w_X)\cdot f_{w_X}(w_X)}{f_{w_Y}(w_Y)}. \tag{34}$$

For a given w_X, the coefficient w_Y will have an identical pdf as the noise coefficient w_N, except that it is translated by w_X. In other words

$$f_{w_Y|w_X}(w_Y|w_X) = f_{w_N}(w_Y - w_X). \tag{35}$$

Substituting (34) and (35) into (33), we can express the wavelet MAP filter as

$$\hat{w}_\sigma = \arg\max_{w_X} f_{w_N}(w_Y - w_X) f_{w_X}(w_X). \tag{36}$$

We have implemented a MAP-filter based on the NIG models for $w_X[x,y]$ and $w_N[x,y]$ discussed previously. In this case, (36) must be solved numerically.

As for the Γ-MAP filter, we want to implement some thresholds for homogeneous regions and strong scatterers. For a homogeneous region (pure speckle) the degree of homogeneity can be expressed as

$$\nu = \frac{E^2\{I|\sigma\}}{\mathrm{var}\{I|\sigma\}} = L. \tag{37}$$

To make the homomorphic Γ-WMAP filter preserve homogeneous regions, we set the wavelet coefficients corresponding to regions where $\nu \ge L$ to zero. Thus, the homomorphic Γ-WMAP filter act as a lowpass filter in homogeneous regions.

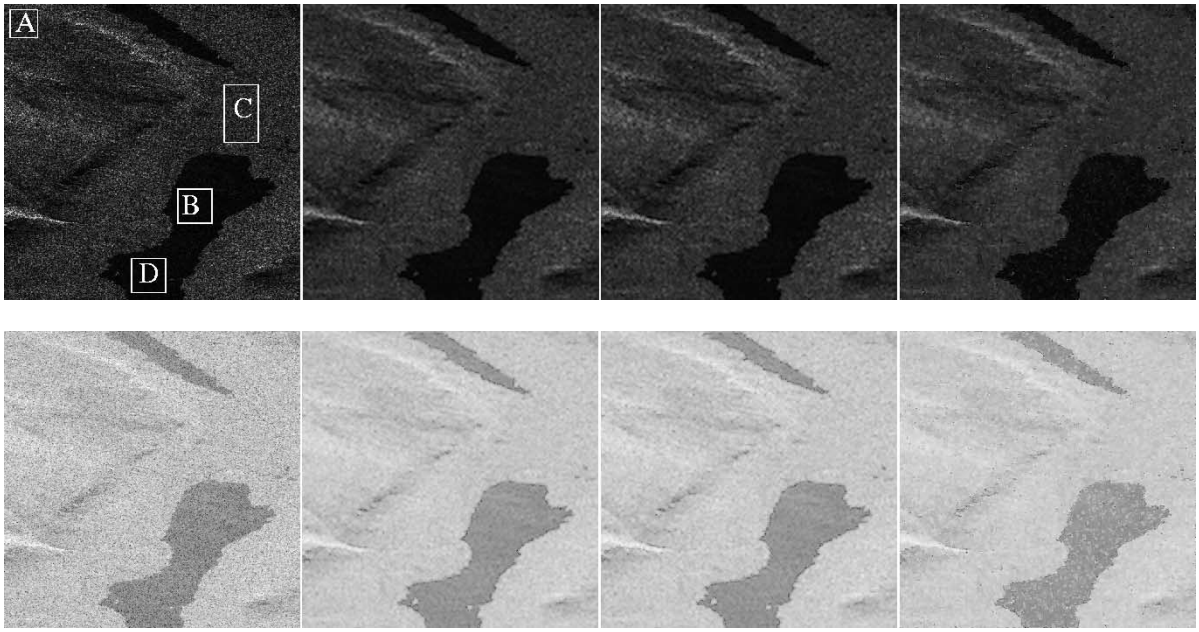

Fig. 5. Original image and the results of the homomorphic-Γ-WMAP, Γ-WMAP and Γ-MAP filters, respectively. The window size is 5 × 5 for all filters. The top row shows the results in amplitude, whereas the bottom row are displayed in decibels. All images are 512 × 512 pixels and displayed in SAR-geometry.

For pixels where the corresponding wavelet coefficient contributions cannot be modeled with NIG-distributions, i.e., (10) is not fulfilled, we assume that the intensity is not K-distributed due to the presence of, for example, strong scatterers. The same assumption is made if (36) has no solution. In these cases, we leave the wavelet coefficients unchanged.

C. Summary of the Despeckling Algorithm

- Make local estimates of the parameters μ_σ and ν from the K-distributed intensity image, using, for example, EM-estimators [33] in a small window centered around pixel $[x, y]$.
- Apply a logarithmic transformation to the intensity image.
- Apply a SWT on the log-transformed intensity image.
- Estimate the four lower order cumulants $\kappa_N^{(n)}$ of the log-transformed speckle $N[x, y]$ from the theoretical models, using (23) and (24).
- Estimate the four lower order cumulants $\kappa_X^{(n)}$ of the log-transformed reflectance $X[x, y]$ using (22). The parameters μ_σ and ν are estimated from data.
- Transform the cumulants of both the log-transformed RCS and the log-transformed speckle into the wavelet domain using (20).
- Estimate the parameters in the corresponding NIG-distributions using the cumulant-based estimator in (9).
- Where $\nu < L$, estimate the wavelet coefficients of a speckle free image using (36). Where $\nu \geq L$, set the wavelet coefficients to zero.
- Apply an inverse SWT and an exponential transform to obtain a speckle-free intensity image.

We note that the above algorithm is completely automatic. That is, no parameters need to be set, except for the size of neighborhood used for estimating μ_σ and ν, and the number of looks L, which is given by the SAR processor.

VI. Despeckling Results

We test the statistical homomorphic wavelet filter on a SAR image covering a mountainous area in Norway. It is a single-look Radarsat image acquired in S7 mode, i.e., incidence angle of about 47°. The scene is shown in Fig. 5 and Fig. 6 and covers parts of the lake Nedre Heimdalvatn and its surroundings. [39].

The filters are tested with respect to the following properties:

- smoothing of homogeneous areas;
- preservation of local mean value;
- statistics of the removed speckle (compared to theoretical model).

All filters are configured equally, i.e., we use an EM-estimator [33] on a neighborhood to estimate the parameters μ_σ and ν. The experiments are repeated with neighborhood sizes of 5 × 5, 7 × 7, and 9 × 9 pixels, respectively. Further, the thresholds of (32) and (37) have been utilized. Both the homomorphic and regular Γ-WMAP filters utilize Daubechies DB2 filter coefficients in the wavelet transform, which is limited to four levels.

SAR images are normally presented in slant-range or SAR-geometry, which do not correspond to a map projection of the ground. Topographic variations in the imaged area introduce geometric distortions. The process of warping SAR data from SAR-geometry to a map projection is known as geocoding [40]. Because geocoding may interpolate and subsample the original image in order to correct for geometric distortions, the process may alter image statistics. Therefore, geocoding has not been performed.

Results of the homomorphic Γ-WMAP, Γ-WMAP and Γ-MAP filters are shown in Figs. 5 and 6 with 5 × 5 and 9 × 9 windows, respectively. We observe that the results of the different filters have similar visual appearance, which is reasonable, since all the filters are based on the same statistical assumptions and all utilize the same neighborhood sizes.

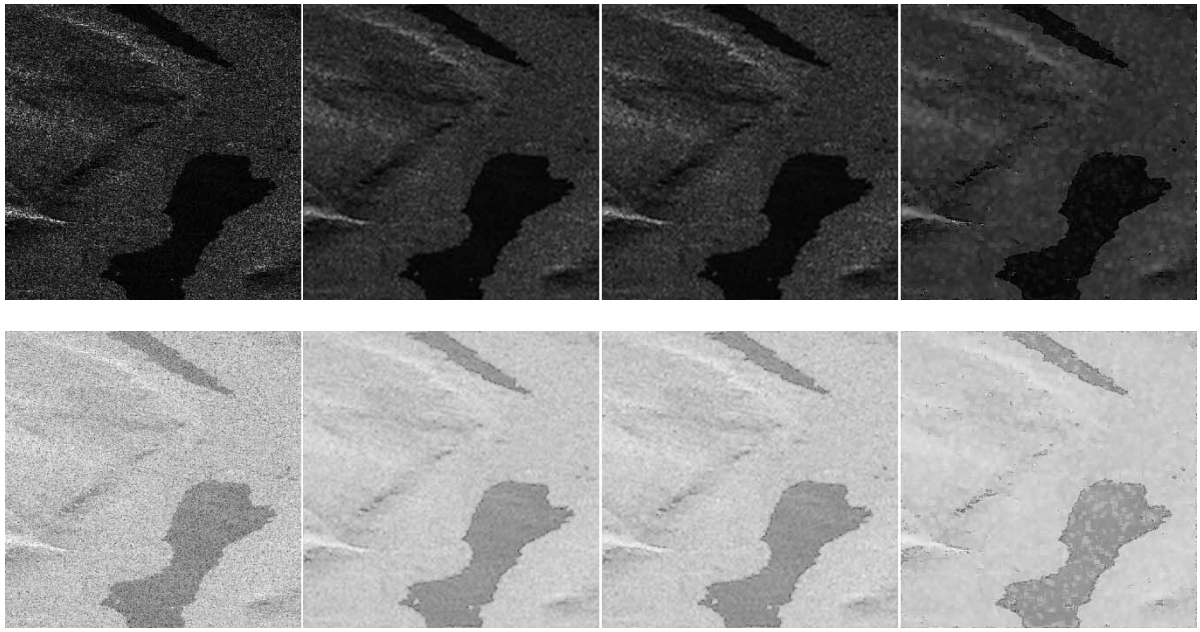

Fig. 6. Original image and the results of the homomorphic-Γ-WMAP, Γ-WMAP, and Γ-MAP filters, respectively. The window size is 9×9 for all filters. The top row shows the results in amplitude, whereas the bottom row are displayed in decibels. All images are 512×512 pixels and displayed in SAR-geometry.

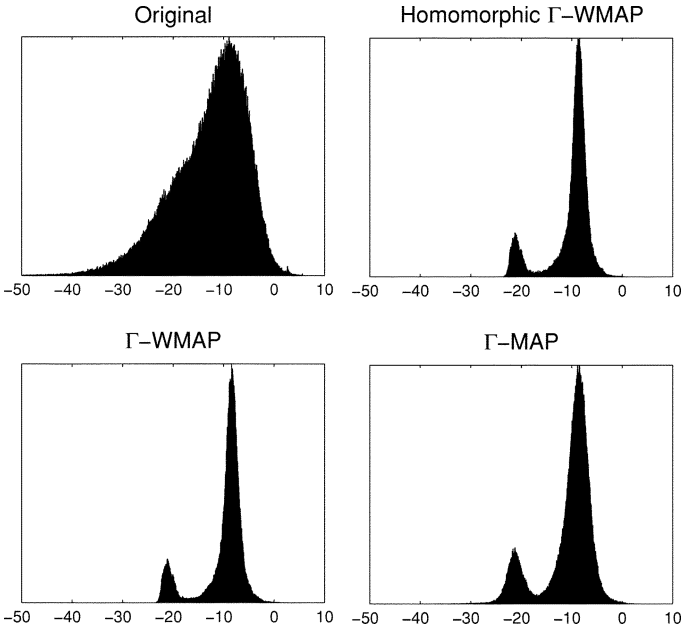

Fig. 7. Histograms of the intensity before and after filtering. The x axis shows intensity in decibels, and the y axis shows normalized histograms. 5×5 neighborhoods are applied in all filters.

We also observe that the different window sizes yield results with similar visual appearance. However, the Γ-MAP filter is observed to produced "blocky" results in some regions. This is especially the case on water surfaces when a 9×9 neighborhood is utilized. The Γ-MAP filter is also observed to preserve strong scatterers better than its wavelet-based counterparts.

Histograms corresponding to the intensity of the image before and after filtering are shown in Fig. 7. All filters are observed to produce similar histograms. The histograms of the filtered images are bimodal. Since the water region in the image has lower intensity than land pixels, it is reasonable to believe that the two modes correspond to pixels mostly located in the water and land regions, respectively. We obsereve that the histograms of the two wavelet-based filters have narrower modes than the histogram of the Γ-MAP filtered image, especially the larger mode corresponding to land. This indicates that wavelet filters yield less variance in the land and water classes.

Tables I–III show measures of homogeneity and bias for the image segments labeled A–D in Fig. 5 with neighborhood sizes of 5×5, 7×7, and 9×9 pixels, respectively. The two measures of homogeneity, which have been used, are the equivalent number of independent looks (ENIL) and the standard deviation of a logarithmic transformed (decibel) intensity image (std-log). The ENIL is defined as

$$\text{ENIL} = \frac{\widehat{E\{I\}}^2}{\widehat{\text{var}\{I\}}} \tag{38}$$

where $\widehat{E\{I\}}$ and $\widehat{\text{var}\{I\}}$ are estimated from a homogeneous area in the despeckled image. We observe that according to the ENIL and std-log numbers the homomorphic Γ-WMAP filter produces smoother results than the other filters. Further, we observe that the smoothing performance of the wavelet-based filters is relatively independent of the size of the window used for estimating μ_σ and ν. The Γ-MAP filter, on the other hand, produces smoother results with increasing estimation windows, for all regions except region A. This is likely to be because the smoothing behavior of the wavelet-based filters is determined by the lowpass filtering properties of the SWT (when all detail wavelet coefficients are shrunk to zero), which depends on the wavelet basis utilized and the overall depth of the transform. The smoothing behavior of the Γ-MAP filter, on the other hand, is determined by the size of the averaging window. Thus, one might claim that this comparison is unfair in favor to the Γ-MAP filter.

TABLE I
RESULTS OF THE DIFFERENT SPECKLE FILTERS WITH 5 × 5 WINDOW SIZE

Image	Region A			Region B			Region C			Region D		
	ENIL	std-log	bias [%]	ENIL	std-log	bias [%]	ENIL	std-log	bias [%]	ENIL	std-log	bias [%]
Original	0.9	5.80	—	1	5.38	—	1	5.72	—	1	5.56	—
H. Γ-WMAP	22.1	0.88	-4.37	50.9	0.61	0.51	61.6	0.55	-3.43	48.5	0.63	0.076
Γ-WMAP	19.4	0.92	0.51	50.8	0.61	0.85	54.8	0.58	0.92	48.1	0.63	0.42
Γ-MAP	6.2	1.78	-4.80	10.7	1.52	-2.44	9.8	1.45	-4.13	11.4	1.36	-2.42

TABLE II
RESULTS OF THE DIFFERENT SPECKLE FILTERS WITH 7 × 7 WINDOW SIZE

Image	Region A			Region B			Region C			Region D		
	ENIL	std-log	bias [%]	ENIL	std-log	bias [%]	ENIL	std-log	bias [%]	ENIL	std-log	bias [%]
Original	0.9	5.80	—	1	5.38	—	1	5.72	—	1	5.56	—
H. Γ-WMAP	22.2	0.88	-4.36	50.8	0.61	0.51	61.6	0.55	-3.43	48.5	0.63	0.076
Γ-WMAP	19.6	0.92	0.48	50.8	0.61	0.85	54.8	0.58	0.92	48.1	0.63	0.42
Γ-MAP	20.2	1.09	-4.48	19.4	1.15	-2.31	18.2	1.03	-2.70	20.2	1.09	-1.80

TABLE III
RESULTS OF THE DIFFERENT SPECKLE FILTERS WITH 9 × 9 WINDOW SIZE

Image	Region A			Region B			Region C			Region D		
	ENIL	std-log	bias [%]	ENIL	std-log	bias [%]	ENIL	std-log	bias [%]	ENIL	std-log	bias [%]
Original	0.9	5.80	—	1	5.38	—	1	5.72	—	1	5.56	—
H. Γ-WMAP	22.2	0.87	-4.36	50.9	0.61	0.51	61.6	0.55	-3.43	48.5	0.63	0.076
Γ-WMAP	19.8	0.92	0.47	50.8	0.61	0.85	54.8	0.58	0.92	48.1	0.63	0.42
Γ-MAP	13.1	1.18	-4.94	27.6	0.89	-1.85	29.3	0.81	-2.31	30.3	0.81	-1.28

According to the results in Tables I and II, all the filters introduce a small bias. The Γ-WMAP filter generally introduces least bias, around 0.5% for all the regions A–D. The Γ-MAP filter generally yields an under bias of a few percent. This is consistent with results reported in [41], for example. The homomorphic Γ-WMAP filter yield a bias as high as −4.36% in region A, whereas it is practically unbiased in region D. Unbiasedness is an important property of speckle filters, especially in applications where radiometric information is important. A typical example is detection of wet snow by change detection in multitemporal SAR data [42].

We note that the ENIL number for area A is a bit below the theoretical value of 1. This may indicate that this area contains some structure, i.e., that it is not completely homogeneous. This also explains why the ENIL numbers for the filtered results are lower in this region than the other regions. The bias in region A introduced by the homomorphic Γ-WMAP and Γ-MAP filters may be a result of the structure present in this region.

Another method of investigating the despeckling performance is to check the ratio between the original and the filtered images. For perfect despeckling, the ratio image should be pure speckle. Thus, its mean should equal one, and its variance should be the inverse of the number of looks [17].

In Table IV, we see the mean and variance for the ratio images, estimated on the image regions A–D of Fig. 5 for all the utilized window sizes.

We observe that the mean of the ratio images for all filters are very close to the theoretical value one. The Γ-MAP filter yields mean value of 1.00 for all regions when 7 × 7 or larger windows are used. However, we observe that the variance of the ratio image produced by the Γ-MAP filter is generally much lower than the corresponding values from the wavelet-based filter. Except for the homomorphic filter in region A, all filters yield ratio images with variances lower than one. This indicate that the filters produce results that follow the original image too closely [17].

TABLE IV
STATISTICS OF THE RATIO BETWEEN THE ORIGINAL AND FILTERED IMAGES

	Filter	A		B		C		D	
		mean	var	mean	var	mean	var	mean	var
5 × 5	H. Γ-WMAP	1.03	1.02	0.98	0.86	1.03	0.98	0.99	0.85
	Γ-WMAP	0.97	0.91	0.98	0.85	0.98	0.87	0.98	0.85
	Γ-MAP	1.00	0.74	1.00	0.73	0.99	0.73	1.00	0.73
7 × 7	H. Γ-WMAP	1.03	1.03	0.98	0.86	1.03	0.98	0.99	0.85
	Γ-WMAP	0.97	0.91	0.98	0.85	0.98	0.87	0.98	0.85
	Γ-MAP	1.00	0.81	1.00	0.79	1.00	0.82	1.00	0.80
9 × 9	H. Γ-WMAP	1.03	1.03	0.98	0.86	1.03	0.98	0.98	0.85
	Γ-WMAP	0.97	0.92	0.98	0.85	0.98	0.87	0.98	0.85
	Γ-MAP	1.01	0.86	1.00	0.86	1.00	0.86	1.00	0.84

As the ENIL and std-log numbers, the results in Table IV indicate that the performance of the wavelet-based filters are relatively independent of the size of the estimation window. In fact, the local means and variances of the ratio images of the homomorphic Γ-WMAP and Γ-WMAP filters do not change with changing window size. On the other hand, the statistics of the ratio image corresponding to the Γ-MAP filter show that this filter depends on the window size. In fact, Table IV shows that the variance tend to increase toward one with increasing window size.

From the mean and variance numbers in Table IV, we also observe that the homomorphic Γ-WMAP filter yields a ratio image that is closer to pure speckle than the ratio image corresponding to the Γ-WMAP image.

VII. Conclusion

In this paper, we have presented the homomorphic Γ-WMAP filter, a wavelet domain statistical speckle filter. The filtering is done by applying the maximum *a posteriori* estimation principle to the wavelet coefficients of a log-compressed SAR image. The filter is a modified version of the Γ-WMAP filter [14] and, hence, relies on the same statistical models for the backscattered signals as the classical Γ-MAP filter. This makes these filters directly comparable. The proposed filter utilizes a logarithmic transformation of the input image in order to model speckle as an additive component, statistically independent of the radar cross section.

The new algorithm is based on modeling the probability density functions of the wavelet coefficients of both the wavelet-transformed reflectance image $w_X[x, y]$ and the wavelet-transformed noise image $w_N[x, y]$ with normal inverse Gaussian distributions. Experiments using synthetic SAR data show that these distributions are excellent models. The parameters in the NIG-distributions can be computed numerically from knowledge of the parameters μ_σ and ν of the K-distribution, which we assume to be the appropriate statistical model for the observed intensity.

The despeckling performance of the proposed algorithm has been studied on a real-world SAR image, and the results have been compared with those of the Γ-MAP and Γ-WMAP filters, for different sizes of the windows used for estimating μ_σ and ν. We have compared the three filters with respect to speckle reduction, introduction of bias and the statistics of removed speckle. We have used the equivalent number of independent looks and std-log to measure the speckle reduction performance. The statistical properties of the filtered outputs have been investigated by comparing the mean and variance ratio images with the theoretical model.

The proposed homomorphic Γ-WMAP filter produces the smoothest results, i.e., removes most speckle, and the removed speckle contribution from this filter has statistics that is closest to the theoretical value. The Γ-WMAP filter generally introduces least bias. The homomorphic Γ-WMAP filter can in some cases introduce a bias of a few percent, which is of the same order as the bias introduced by the Γ-MAP filter.

In fact, the experiments show that MAP filtering of the wavelet coefficients of logarithmic transformed SAR images does not introduce considerable bias, as long as the MAP filtering scheme is based on the parameters μ_σ and ν that are estimated from the intensity image itself. Thus, the proposed homomorphic filter does not suffer from introduction of severe bias, which is reported to happen with wavelet coefficient shrinkage of logarithmically transformed SAR images [12], [21]

The comparison between the Γ-WMAP filter and its homomorphic cousin indicates that using the logarithmic transform to get the speckle contribution additive (compared to handling speckle as an additive but statistically dependent term) has the advantage of slightly increasing the speckle reduction performance, although a small bias may be introduced in some cases. Further, the statistical properties of the removed speckle from the homomorphic Γ-WMAP filter are closer to the theoretical model than for the Γ-WMAP filter.

The Γ-WMAP and homomorphic Γ-WMAP filters are both more computationally demanding than the Γ-MAP filter. This is mainly because the MAP equation for the wavelet coefficients has to be solved numerically, typically with an iterative method. Further, the number of coefficients in the SWT increases with the transform depth. The required number of floating-point operations for an efficiently implemented (homomorphic) Γ-WMAP filter will typically be a factor 100 higher than that of a Γ-MAP filter.

Acknowledgment

The authors want to acknowledge the anonymous reviewers for their thorough review of the manuscript. Their comments and suggestions have greatly improved the quality of the paper. The authors also would like to thank T. Guneriussen (University of Tromsø) for helpful comments. The Radarsat data have been acquired as part of the ADRO project no. 172. Radarsat data are copyright by the Canadian Space Agency 1997.

References

[1] J. W. Goodman, "Some fundamental properties of speckle," *J. Opt. Soc. Amer.*, vol. 66, no. 11, pp. 1145–1150, Nov. 1976.

[2] J. Lee, "Refined filtering of image noise using local statistics," *Comput. Graph. Image Process.*, vol. 15, pp. 255–269, 1981.

[3] ——, "Speckle suppression and analysis for synthetic aperture radar images," *Opt. Eng.*, vol. 25, pp. 636–643, 1986.

[4] D. T. Kuan, A. A. Sawchuck, T. C. Strand, and P. Chavel, "Adaptive noise smoothing filter for images with signal dependent noise," *IEEE Trans. Pattern Anal. Machine Intell.*, vol. PAMI-7, pp. 165–177, 1985.

[5] A. Lopès, E. Nezry, R. Touzi, and H. Laur, "Maximum a posteriori speckle filtering and first order texture models in SAR images," in *Proc. IGARSS*, Washington, DC, 1990, pp. 2409–2412.

[6] M. Vetterli and J. Kovacevic, *Wavelets and Subband Coding*. Upper Saddle River, NJ: Prentice-Hall, 1995.

[7] D. L. Donoho, "De-noising by soft-thresholding," *IEEE Trans. Inform. Theory*, vol. 41, pp. 613–627, May 1995.

[8] H. Guo, J. E. Odegard, M. Lang, R. A. Gopinath, I. W. Selesnick, and C. S. Burrus, "Wavelet based speckle reduction with application to SAR based ATD/R," in *IEEE Proc. Int. Conf. Image Processing*, vol. 1, 1994, pp. 75–79.

[9] L. Gagnon and A. Jouan, "Speckle filtering of SAR images—A comparative study between complex-wavelet-based and standard filters," in *Proc. SPIE Conf. Wavelet Applications Signal Image Processing V*. Bellingham, WA: SPIE, 1997.

[10] S. Fukuda and H. Hirosawa, "Suppression of speckle in synthetic aperture radar images using wavelet," *Int. J. Remote Sens.*, vol. 19, no. 3, pp. 507–519, 1998.

[11] R. Yu, A. R. Allen, and J. Watson, "An optimal wavelet thresholding method for speckle noise reduction," in *Summer School on Wavelets*. Gliwice, Poland: Silesian Tech. Univ., 1996, pp. 77–81.

[12] E. Hervet, R. Fjørtoft, P. Marthon, and A. Lopès, "Comparison of wavelet-based and statistical speckle filters," *Proc. SPIE*, vol. 3497, 1998.

[13] Y. Dong, B. C. Forster, A. K. Milne, and G. A. Morgan, "Speckle suppression using recursive wavelet transforms," *Int. J. Remote Sens.*, vol. 19, no. 2, pp. 317–330, 1998.

[14] S. Solbø and T. Eltoft, "Γ-WMAP: A statistical speckle filter operating in the wavelet domain," *Int. J. Remote Sens.*, vol. 25, no. 5, pp. 1019–1036, Mar. 2004.

[15] S. Foucher, G. B. Bénié, and J.-M. Boucher, "Multiscale MAP filtering of SAR images," *IEEE Trans. Image Processing*, vol. 10, pp. 49–60, Jan. 2001.

[16] F. Argenti and L. Alparone, "Speckle removal from SAR images in the undecimated wavelet domain," *IEEE Trans. Geosci. Remote Sensing*, vol. 40, pp. 2363–2374, Nov. 2002.

[17] C. Oliver and S. Quegan, *Understanding Synthetic Aperture Radar Images*. Norwell, MA: Artech House, 1998.
[18] O. E. Barndorff-Nielsen, "Normal inverse Gaussian distributions and stochastic volatility modeling," *Scan. J. Statist.*, vol. 24, pp. 1–13, 1997.
[19] C. J. Oliver, "Information from SAR images," *J. Phys. D*, vol. 24, no. 6, pp. 1493–1514, 1991.
[20] T. Eltoft and K. A. Høgda, "Non-Gaussian signal statistics in ocean SAR imagery," *IEEE Trans. Geosci. Remote Sensing*, vol. 36, pp. 562–575, Mar. 1998.
[21] A. Bijaoui, Y. Bobichon, Y. Fang, and F. Rue, "Méthodes multiéchelles appliquées à l'analyze des images radar à ouverture synthétique," *Trait. Signal*, vol. 14, no. 2, 1997.
[22] S. Fukuda and H. Hirosawa, "Smoothing effect of wavelet-based speckle filtering: The Haar basis case," *IEEE Trans. Geosci. Remote Sensing*, vol. 37, pp. 1168–1172, Mar. 1999.
[23] R. Fjørtoft and A. Lopès, "Estimation of the mean radar reflectivity from a finite number of correlated samples," *IEEE Trans. Geosci. Remote Sensing*, vol. 39, pp. 196–199, Jan. 2001.
[24] H. Xie, L. E. Pierce, and F. T. Ulaby, "Statistical properties of logarithmically transformed speckle," *IEEE Trans. Geosci. Remote Sensing*, vol. 40, pp. 721–727, Mar. 2002.
[25] G. Strang and T. Nguyen, *Wavelets and Filterbanks*. Cambridge, MA: Wellesey-Cambridge, 1996.
[26] G. P. Nason and B. W. Silverman, "The stationary wavelet transform and some statistical applications," Univ. Bristol, Bristol, U.K., Tech. Rep. BS8 1Tw, 1995.
[27] O. E. Barndorff-Nielsen, "Normal inverse Gaussian processes and the modeling of stock returns," Dept. Theoretical Statist., Inst. Math., Univ. Aarhus, Aarhus, Denmark, Res. Rep. 300, 1995.
[28] A. Hanssen and T. A. Øigrånd, "The normal inverse gaussian distribution as a flexible model for heavy tailed processes," in *Proc. IEEE EURASIP Workshop on Nonlinear Signal and Image Processing*, 2001.
[29] E. Nezry, A. Lopès, D. Ducrot-Gambart, C. Nezry, and J.-S. Lee, "Supervised classification of K-distributed SAR images of natural targets and probabillity of error estimation," *IEEE Trans. Geosci. Remote Sensig*, vol. 34, pp. 1233–1242, Sept. 1996.
[30] E. Jakeman and P. N. Pusey, "Significance of K distributions in scattering experiments," *Phys. Rev. Lett.*, vol. 40, no. 9, pp. 546–550, 1978.
[31] D. R. Iskander, A. M. Abdelhak, M. Zoubir, and B. Boashash, "A method for estimating the parameters of the K distribution," *IEEE Trans. Signal Processing*, vol. 47, pp. 1147–1151, Apr. 1999.
[32] I. R. Joughin, D. B. Percival, and D. P. Winebrenner, "Maximum likelihood estimation of K distribution parameters for SAR data," *IEEE Trans. Geosci. Remote Sensing*, vol. 31, pp. 989–999, Sept. 1993.
[33] W. J. J. Roberts and S. Furui, "Maximum likelihood estimation of K-distribution parameters via the expectation-maximization algorithm," *IEEE Trans. Signal Processing*, vol. 48, pp. 3303–3306, Dec. 2000.
[34] R. Smolíková, M. P. Wachowiak, J. M. Zurada, and A. S. Elmaghraby, "A neural network approach for estimating large K distribution parameters," in *Proc. Int. Joint Conf. Neural Netwoks*, Washington DC, July 2001.
[35] E. P. Simoncelli and E. H. Adelson, "Noise removal via Bayesian wavelet coring," in *Proc. 3rd IEEE Int. Conf. Image Processing*, Lusanne, Switzerland, Sept. 1996.
[36] C. L. Nikias and A. P. Petropulu, *Higher-order Spectra Analysis: A Nonlinear Signal Processing Framework*. Upper Saddle River, NJ: Prentice-Hall, 1993.
[37] J. R. Michael, "The stabilized probability plot," *Biometrica*, vol. 70, no. 1, pp. 11–17, 1983.
[38] R. Fjørtoft, A. Lopès, and F. Adragna, "Radiometric and spatial aspects of speckle filtering," in *Proc. IGARSS*, Honolulu, HI, 2000.
[39] T. Guneriussen, H. Johnsen, and I. Lauknes, "Snow cover mapping capabilities using RADARSAT standard mode data," *Can. J. Remote Sens.*, vol. 27, no. 2, pp. 109–117, 2001.
[40] H. Johnsen, I. Lauknes, and T. Guneriussen, "Geocoding of fast-delivery ERS-1 SAR image mode product using DEM data," *Int. J. Remote Sens.*, vol. 16, no. 11, pp. 1957–1968, 1995.
[41] Z. Shi and K. B. Fung, "A comparison of digital speckle filters," in *Proc. IGARSS*, Pasadena, CA, 1994, pp. 2129–2133.
[42] T. Nagler and H. Rott, "Retrieval of wet snow by means of multitemporal SAR data," *IEEE Trans. Geosci. Remote Sensing*, vol. 38, pp. 754–765, Mar. 2000.

Stian Solbø received the M.E. degree from the University of Tromsø, Tromsø, Norway, in 2001, where he is currently pursuing the Ph.D. degree.

In 2002, he joined Norut Information Technology Ltd. as a Research Scientist, where he is currently working on flood monitoring and automatic detection of surface water from SAR images. His main research interests are remote sensing, pattern recognition, and statistical signal processing.

Torbjørn Eltoft (A'93–M'98) received the Cand.Real. (M.S.) and Dr.Scient. (Ph.D.) degrees from the University of Tromsø, Tromsø, Norway, in 1981 and 1984, respectively.

His early research was on the application of modern signal processing techniques in experimental ionospheric physics. Since 1984, he has been working with remote sensing, with special interest in the nonlinear SAR-imaging of ocean waves, and scattering of microwaves from the ocean surface. He joined the Department of Physics, University of Tromsø in 1988, where he is currently a Professor in the Group of Electrical Engineering. He is currently also affiliated with Norut IT Ltd., Tromsø, as an Adjunct Professor. His current research interests are remote sensing, image and signal processing, and artificial neural networks.

Dr. Eltoft, together with Prof. Rui de Figuiredo, University of California, Irvine, was awarded the year 2000 Outstanding Paper Award in Neural Networks by the IEEE Neural Networks Council.